The nuclear quadrupole coupling constants and the structure of the *para–para* ammonia dimer

N. Heineking and W. Stahl
Institut für Physikalische Chemie, Christian-Albrechts-Universität, D-24098 Kiel, Germany

E. H. T. Olthof, P. E. S. Wormer, and A. van der Avoird
Institute of Theoretical Chemistry, Nijmegen-SON Research Center, University of Nijmegen, Toernooiveld, 6525 ED Nijmegen, The Netherlands

M. Havenith
Institut für Angewandte Physik, Wegelerstrasse 8, D-53115 Bonn, Germany

Expressions are derived for the nuclear quadrupole splittings in the E_3 and E_4 (*para–para*) states of $(NH_3)_2$ and it is shown that these can be matched with the standard expressions for rigid rotors with two identical quadrupolar nuclei. The matching is exact only when the off-diagonal Coriolis coupling is neglected. However, the selection rules for rotational transitions are just opposite to those for the rigid rotor. Hyperfine splittings are measured for the $J=2\leftarrow 1$ transitions in the E_3 and E_4 states with $|K|=1$; the quadrupole coupling constants $\chi_{aa}=0.1509(83)$ MHz and $\chi_{bb}-\chi_{cc}=2.8365(83)$ MHz are extracted from these measurements by the use of the above mentioned correspondence with the rigid rotor expressions. The corresponding results are also calculated, with and without the Coriolis coupling, from the six-dimensional vibration–rotation–tunneling (VRT) wave functions of $(NH_3)_2$, which were previously obtained by Olthof *et al.* [E.H.T. Olthof, A. van der Avoird, and P.E.S. Wormer, J. Chem. Phys. **101**, 8430 (1994)]. From the comparison of χ_{aa} with the measured value it follows that the semiempirical potential and the resulting VRT states of Olthof *et al.* are very accurate along the interchange $(\vartheta_A,\vartheta_B)$ coordinate. From $\chi_{bb}-\chi_{cc}$ it follows that this potential is probably too soft in the dihedral angle $\bar{\gamma}=\gamma_A-\gamma_B$, which causes the torsional amplitude to be larger than derived from the experiment. © *1995 American Institute of Physics.*

I. INTRODUCTION

For about 20 years the ammonia dimer has been the subject of several studies addressing the question whether $(NH_3)_2$ is a hydrogen bonded complex. Most of the earlier *ab initio* calculations had led to the conclusion that the ammonia dimer has a hydrogen bonded equilibrium structure.[1–6] In 1985, however, Nelson *et al.*[7,8] deduced a structure from microwave measurements, which contradicts this prediction. They found that the C_3 axes of the NH_3 monomers make nearly complementary angles with the intermolecular axis: the cyclic (antiparallel) structure. The determination of this structure was based on measurements of the hyperfine splittings and the Stark effect in two tunneling states. These two tunneling states were assigned as G states in the symmetry group G_{36}, which can be viewed either as states with one unit of angular momentum associated with one internal rotor (the *para* monomer) and zero internal angular momentum associated with the other rotor (the *ortho* monomer) or as two interchange tunneling partners.[9] This interchange implies that the two monomers exchange their roles as proton donor and acceptor in the hydrogen bond.

In a later far-infrared study[10] several tunneling levels were probed, but since none of them shared a common level, no information concerning the dynamics of the complex could be extracted. The ground states of the transitions observed in the far-infrared region[10] were probed in an infrared–far-infrared double resonance experiment by Havenith *et al.*[11] This study, as well as an extensive far-infrared

study by Loeser *et al.*[12] and a theoretical study by van Bladel *et al.*[13] led to the following conclusions: (i) The two tunneling G levels probed by Nelson *et al.* are the two partially quenched umbrella inversion components (Nelson *et al.* had assumed that the umbrella inversion of the NH_3 monomers in the complex is quenched). As a consequence, the appropriate symmetry group must be extended to G_{144} and the G levels of G_{36} split into $G_2^{\pm}$ levels of G_{144}. (ii) The interchange tunneling splitting was found to be large (about 480 GHz). As a consequence, the high barrier limit does not apply, and large amplitude internal motion is expected. Therefore, vibrational averaging effects can contribute substantially and the structure deduced from the measurements of Nelson *et al.* does not have to agree with the equilibrium structure. However, in the study by Nelson *et al.*[7,8] it was found that the relevant monomer orientations, as probed by the dipole moment and the nuclear quadrupole coupling constants, hardly change upon isotope substitution. Hence, these authors concluded that $(NH_3)_2$ is nearly rigid and that the nearly cyclic structure must coincide with the equilibrium structure.

Further experiments on different tunneling states which probed different parts of the potential surface helped to solve these issues. Linnartz *et al.*[14] measured the Stark effect, i.e., the axial component of the dipole moment, in the $G_2^{\pm}$ states with $|K|=1$, which gives direct information on the orientations of the monomers in this state. This study demonstrated clearly the effect of vibrational averaging. Whereas for the

$G_2^\pm$ states with $K=0$ the dipole moment was found to be 0.74 D,[7] a value of only 0.10 D was obtained for the $G_2^\pm$ states with $|K|=1$. Incidentally, it might be noted that for a rigid structure with a linear hydrogen bond a dipole moment of about 2.0 D is expected. The small dipole implies that averaged over the time scale of the experiment the complex reflects a nearly antiparallel, cyclic structure. Two recent *ab initio* studies led to different predictions of the equilibrium structure: whereas Hassett *et al.*[15] found a hydrogen bonded structure, Tao and Klemperer[16] found the cyclic structure.

A recent series of studies by Olthof *et al.*[17–20] presents a theoretical approach to these issues. They constructed a family of model potentials with different barriers in the interchange motion and in the hindered rotations of the two NH_3 monomers around their C_3 axes. For each of these potentials they calculated the six-dimensional vibration–rotation–tunneling (VRT) states of $(NH_3)_2$ and the expectation values of the dipole moment and the hyperfine splittings. By improving the parameters they arrived at a model potential that was able to reproduce all the observed far-infrared frequencies [10,12] with deviations of only about 1% and that gives good agreement for all values of the dipole moment and the nuclear quadrupole splittings observed so far. Even the very small splittings due to the hindered umbrella inversions could be quantitatively computed[20] from the VRT states calculated in Ref. 19. In calculations of the VRT states and the properties of $(ND_3)_2$ the observed[7,8] effects of isotope substitution were also quantitatively reproduced.[19] The discussion whether the ammonia dimer is hydrogen bonded could thus be concluded. The potential minimum is found to correspond to a strongly bent hydrogen bonded structure, and the donor–acceptor interchange barrier is very low (about 7 cm^{-1}). The criteria implied in the term hydrogen bonding: strong directionality and near linearity, are not met in the case of $(NH_3)_2$. Also the apparent contradictions in the experimental observations could be explained. VRT states with different symmetries or different (approximate) K quantum numbers show substantial differences in their averaged properties. The influence of isotope substitution in the G states probed by Nelson *et al.*[7,8] is rather unexpected: the calculations[19] showed that the average structure of $(NH_3)_2$ is closer to equilibrium than the average structure of $(ND_3)_2$. This appears to be caused by the different internal rotor behavior of *ortho* and *para* ammonia monomers.

As an important test for the newly established potential of Olthof *et al.* we present the measurement of pure rotational transitions in the E_3 and E_4 *para–para* states of $(NH_3)_2$ with $|K|=1$, with fully resolved hyperfine structure. We compare the hyperfine coupling constants with the results of calculations based on the potential of Olthof *et al.* The measurements were carried out on the pulsed molecular beam Fourier transform microwave spectrometer in Kiel. These measurements probe the orientations of the NH_3 monomers, for the first time in a state which is not a mixed *ortho–para* (G) state. So far, no experimental information was available on the dihedral angle between the C_3 axes. In the study of Nelson *et al.* it was always assumed, due to this lack of information, that the monomer C_3 axes lie in one plane. Also the more recent experiments[10–12,14] do not di-

rectly probe the out of plane motion. Therefore, it may be asked how accurate the model potential developed by Olthof *et al.* is in its dependence on the dihedral angle. Our measurement probes the out of plane motion of the complex by the determination of the perpendicular component of the hyperfine coupling $\chi_{bb} - \chi_{cc}$, in addition to the parallel component χ_{aa}.

The observed hyperfine splittings of the E_3 and E_4 states with $|K|=1$ are fitted by a computer program meant for rigid rotors. In this procedure the ammonia dimer is treated as if it were a rigid prolate symmetric top. As discussed above, the dimer is not at all rigid. In Sec. II it will be shown, however, that the expressions for the quadrupole splittings in the E_3 and E_4 states of $(NH_3)_2$ can be matched with the standard rigid rotor expressions. The agreement is exact only when the (weak) off-diagonal Coriolis coupling is neglected, i.e., when K is assumed to be an exact quantum number. From this derivation it follows, at the same time, that the selection rules for rotational transitions in the E_3 and E_4 states of the $(NH_3)_2$ dimer are just opposite to the rigid rotor selection rules. In Sec. III we briefly describe the experimental setup and in Sec. IV we present the measured hyperfine coupling constants and the corresponding results calculated with and without Coriolis coupling. Finally, in Sec. V, we discuss what can be learned from the comparison between the experimental and calculated results.

II. THEORY

The splitting of the E_3 and E_4 levels with $|K|=1$ into nine sublevels by the interaction with the electric quadrupoles of the ^{14}N nuclei, can be described by a formalism which is very similar to the usual theory[21] for rigid prolate symmetric tops, provided we neglect the off-diagonal Coriolis interaction. The explanation of this fact will be the subject of this section.

The coordinate system used is described in detail in Ref. 17. In short, the vector **R**, connecting the centers of mass of the monomers A and B, has polar coordinates R,β,α with respect to an arbitrary space-fixed frame. A two-angle embedded dimer frame is chosen such that its z axis is along **R**. With respect to this frame the principal axes frames of the monomers have Euler angles γ_X, ϑ_X and φ_X, $X=A,B$. The angles ϑ_X and γ_X are the polar angles of the monomer C_3 axes, the angles φ_X describe the rotations of the monomers about their C_3 axes. Later we will use $\gamma = \frac{1}{2}(\gamma_A + \gamma_B)$ as an external angle, i.e., an overall rotation angle of the dimer, together with β and α, and the dihedral angle $\bar{\gamma} = \gamma_A - \gamma_B$ as an internal angle.

A. The rigid rotor with two identical quadrupolar nuclei

Let us first describe briefly the quadrupole splitting in the dimer from the perspective of rigid rotor theory. We will follow Ref. 21 as closely as possible. We choose the a axis along z (the long axis), the b axis along x, and the c axis along y. The operator describing the coupling with nucleus N_X is a term in the multipole expansion of the Coulomb interaction between N_X and the other charged particles in the dimer, which we write in irreducible tensor notation as

$$H_{qQ} = \sum_{X=A,B} \boldsymbol{q}^X \cdot \boldsymbol{Q}^X = \sum_X \sum_\mu (-1)^\mu q^X_{-\mu} Q^X_\mu, \qquad (1)$$

where the tensors are expressed with respect to the space-fixed frame. The irreducible tensor $\boldsymbol{Q}^X$ is the quadrupole of nucleus N_X. The second rank irreducible gradient tensor $\boldsymbol{q}^X$ is related to the field gradient tensor $\bar{\boldsymbol{q}}^X$ expressed with respect to the dimer frame by

$$q^X_\mu = \sum_\nu D^{(2)}_{\mu\nu}(\alpha,\beta,\gamma)^* \bar{q}^X_\nu. \qquad (2)$$

The quantities $D^{(2)}_{\mu\mu'}$ are elements of Wigner D matrices in the active convention of, e.g., Ref. 22.

Let us indicate the nitrogen nuclear spins by I_A (= 1) and I_B (= 1), which we Clebsch–Gordan couple as follows:

$$|\mathscr{T}M_{\mathscr{T}}\rangle = \sum_{M_A M_B} |I_A M_A\rangle |I_B M_B\rangle \langle I_A M_A ; I_B M_B | \mathscr{T}M_{\mathscr{T}}\rangle,$$

$$\mathscr{T} = 0,1,2. \qquad (3)$$

If we were to neglect the hyperfine interaction, the total angular momentum J of the dimer would be a constant of the motion. The conservation of J is broken by the quadrupole coupling to the nitrogen nuclei, which, however, is so small that only first-order mixing has to be considered, i.e., we take a fixed value $J' = J$. So, we couple $\mathscr{T}$ and J to a resultant angular momentum F that is a strict constant of the motion.

The following matrix element, arising in a first-order treatment, can be evaluated by repeated application of the Wigner–Eckart theorem, cf. Ref. 21, Eqs. (15.117) and (15.118). We assume that the field gradient tensors at the two nitrogen nuclei are equal when expressed in the monomer frames. Furthermore, we will see below that, due to the interchange symmetry of the two interacting *para* monomers, they are also equal in the dimer frame. This implies that the reduced matrix elements of the field gradient of A and B are equal. The nuclear quadrupole is determined by the nucleons and is not affected by the environment outside the nucleus, so that the reduced matrix elements of the quadrupoles are also equal. Hence we find

$$H_{\mathscr{T}'\mathscr{T}} \equiv \langle \tau',(J\mathscr{T}')FM_F | H_{qQ} | \tau,(J\mathscr{T})FM_F \rangle$$

$$= \langle \tau',J\|q^A\|\tau,J\rangle \langle I_A\|Q^A\|I_A\rangle \sum_X \sum_{M'_A,M'_B} \sum_{M'_{\mathscr{T}},M'_J} \sum_{M_A,M_B} \sum_{M_{\mathscr{T}},M_J} \langle FM_F | JM'_J ; \mathscr{T}'M'_{\mathscr{T}}\rangle$$

$$\times \langle \mathscr{T}'M'_{\mathscr{T}} | I_A M'_A ; I_B M'_B\rangle \sum_\mu (-1)^\mu \langle JM'_J | 2,-\mu ; JM_J\rangle \langle I_X M'_X | 2,\mu ; I_X M_X\rangle \langle I_A M_A ; I_B M_B | \mathscr{T}M_{\mathscr{T}}\rangle \langle JM_J ; \mathscr{T}M_{\mathscr{T}} | FM_F \rangle$$

$$= (-1)^{t_1}[1+(-1)^{\mathscr{T}'-\mathscr{T}}][(2\mathscr{T}+1)(2\mathscr{T}'+1)]^{1/2} \langle \tau',J\|q^A\|\tau,J\rangle \langle I_A\|Q^A\|I_A\rangle \begin{Bmatrix} F & \mathscr{T}' & J \\ 2 & J & \mathscr{T} \end{Bmatrix} \begin{Bmatrix} I_A & \mathscr{T}' & I_B \\ \mathscr{T} & I_A & 2 \end{Bmatrix}, \qquad (4)$$

where $t_1 = \mathscr{T}' + \mathscr{T} + J + F$ and the reduced matrix elements can be calculated from

$$\langle \tau',J\|q^A\|\tau,J\rangle = f(J)\langle \tau',J,M_J=J | q^A_0 | \tau,J,M_J=J\rangle$$

$$\equiv f(J)\langle \tau',J,J | q^A_0 | \tau,J,J\rangle,$$

$$\langle I_A\|Q^A\|I_A\rangle = f(I_A)\langle I_A,M_A=I_A | Q^A_0 | I_A,M_A=I_A\rangle \qquad (5)$$

$$\equiv f(I_A)\langle I_A,I_A | Q^A_0 | I_A,I_A\rangle.$$

The expressions between curly brackets are $6j$ symbols and $f(J)$ is the inverse of a $3j$ symbol,

$$f(J) = \left[2 \begin{pmatrix} J & 2 & J \\ J & 0 & -J \end{pmatrix} \right]^{-1}.$$

The factor 2 is by convention. The quantum numbers τ and τ' stand for the remaining quantum numbers necessary to label the states completely; they do not enter the Wigner–Eckart theorem. The expectation value of the nuclear quadrupole operator Q^A_0 is simply

$$\langle I_A,I_A | Q^A_0 | I_A,I_A\rangle = eQ ,$$

where eQ is the nuclear quadrupole moment of ^{14}N. The field gradient matrix element is often designated by

$$\langle \tau',J,J | q^A_0 | \tau,J,J\rangle = q_J.$$

The factor $[1+(-1)^{\mathscr{T}'-\mathscr{T}}]$ is zero or two, and expresses the fact that $\mathscr{T}$ and $\mathscr{T}'$ must be simultaneously odd or even. The nine-dimensional first-order matrix $H_{\mathscr{T}'\mathscr{T}}$ is almost completely diagonal, the only off-diagonal element being between states with $\mathscr{T}'=2$, $\mathscr{T}=0$ and $\mathscr{T}'=0$, $\mathscr{T}=2$.

Our computer program that fits the reduced matrix elements to the observed splittings is based on asymmetric top functions: $|\tau,J\rangle \equiv |\lambda,J_{K_a K_c}\rangle$, where λ labels the "internal" part of the wave function. By insertion of Eq. (2) and use of

$$D^{(2)}_{0\nu}(\alpha,\beta,\gamma)^* = (-1)^\nu C^{(2)}_\nu(\beta,\gamma),$$

where $C^{(2)}_\nu$ is a spherical harmonic function normalized to $4\pi/5$, we obtain

$$eQq_J = eQ\langle \tau', J, J \mid q_0^A \mid \tau, J, J\rangle$$

$$= \sum_{\nu} (-1)^{\nu} \langle J_{K_a K_c} \mid C_{\nu}^{(2)}(\beta, \gamma) \mid J_{K_a K_c}\rangle \chi_{\nu}. \tag{6}$$

In Sec. II B we will derive explicit expressions for

$$\chi_{\nu} = eQ\bar{q}_{\nu}^A = eQ\bar{q}_{\nu}^B$$

as matrix elements of $C_{\nu}^{(2)}(\vartheta_X, \gamma_X)$ over the internal part of the wave functions of $(NH_3)_2$. Here, we consider this complex as a rigid rotor and we treat the components χ_{ν} of the quadrupole coupling tensor as parameters which must be extracted from the experimentally observed hyperfine splittings. Equation (6) is in complex spherical form; often it is written in real spherical form. The "Vierergruppe" $V(a,b,c)$ is a symmetry group of the asymmetric top, see Ref. 21, p. 405. It is easy to show that only the real operators $C_0^{(2)}$ and $C_2^{(2)} + C_{-2}^{(2)}$ transform according to A_1 of $V(a,b,c)$ and hence only those contribute nonvanishing diagonal matrix elements to eQq_J in Eq. (6).

Introducing the direction cosines Φ_{Zg} of the a, b, and c axes with respect to the space-fixed Z axis,

$$\Phi_{Za} = \cos\beta, \quad \Phi_{Zb} = \sin\beta\cos\gamma, \quad \Phi_{Zc} = \sin\beta\sin\gamma,$$

and observing that the field gradient tensor χ is traceless and symmetric, we can easily show that

$$\sum_{g=a,b,c} \Phi_{Zg}^2 \chi_{gg} = C_0^{(2)}(\beta,\gamma)\chi_{aa} + \frac{1}{\sqrt{6}}[C_2^{(2)}(\beta,\gamma)$$

$$+ C_{-2}^{(2)}(\beta,\gamma)](\chi_{bb} - \chi_{cc}). \tag{7}$$

This enables us to write Eq. (6) as follows:

$$eQq_J = \sum_{g=a,b,c} \langle J_{K_a K_c} \mid \Phi_{Zg}^2 \mid J_{K_a K_c}\rangle \chi_{gg}, \tag{8}$$

where the tensor χ is now in Cartesian form. Comparison of the real equivalent of Eq. (6) with Eq. (8) shows the connection between the Cartesian components χ_{gg} and the spherical components χ_{ν} of χ.

If the asymmetric rotor becomes a prolate symmetric top, one finds the following relation between the wave functions:

$$|J_{K_a K_c}\rangle \rightarrow [|J,K\rangle + (-1)^{J+K_a+K_c}|J,-K\rangle]/\sqrt{2} \tag{9}$$

with $K = K_a$. The correlation is based on the fact that the left- and right-hand side of Eq. (9) transform according to the same irreducible representation of $V(a,b,c)$. The kets in Eq. (9) are the usual symmetric top functions

$$|J,K\rangle = \left(\frac{2J+1}{8\pi^2}\right)^{1/2} D_{JK}^{(J)}(\alpha,\beta,\gamma)^*. \tag{10}$$

Substitution of Eqs. (7) and (9) into (8) yields

$$eQq_J = \frac{1}{2}[\langle J,K|C_0^{(2)}|J,K\rangle + \langle J,-K|C_0^{(2)}|J,-K\rangle]\chi_{aa}$$

$$+ \frac{1}{2\sqrt{6}}(-1)^{J+K_a+K_c}[\langle J,K|C_2^{(2)}|J,-K\rangle$$

$$+ \langle J,-K|C_{-2}^{(2)}|J,K\rangle](\chi_{bb} - \chi_{cc}). \tag{11}$$

Using the pairwise equality of the rotational matrix elements, we find

$$eQq_J = \langle J,K|C_0^{(2)}(\beta,\gamma)|J,K\rangle\chi_{aa} + \frac{1}{\sqrt{6}}(-1)^{J+K_a+K_c}$$

$$\times \langle J,K|C_2^{(2)}(\beta,\gamma)|J,-K\rangle(\chi_{bb} - \chi_{cc}). \tag{12}$$

Note the appearance of the term with $\nu=2$; it would be missing if because of symmetry $\chi_{bb} = \chi_{cc}$. In the ammonia dimer states with $|K|=1$ this term is present.

Often Eq. (12) is written in terms of equivalent operators. We use the Wigner–Eckart theorem and find that

$$\langle J,K'|C_0^{(2)}|J,K\rangle = [(2J+3)(J+1)]^{-1}\langle J,K'|3\hat{J}_a^2 - \hat{J}^2|J,K\rangle$$

and

$$\langle J,K'|C_{\pm2}^{(2)}|J,K\rangle = \frac{1}{2}\sqrt{6}[(2J+3)(J+1)]^{-1}\langle J,K'|\hat{J}_{\pm}^2|J,K\rangle.$$

We can then easily show that

$$eQq_J = \frac{J}{2J+3}[\chi_{aa}D_1 + (\chi_{bb} - \chi_{cc})D_2] \tag{13}$$

with

$$D_1 = \frac{1}{J(J+1)}(3\langle\hat{J}_a^2\rangle - \langle\hat{J}^2\rangle) \tag{14}$$

and

$$D_2 = \frac{1}{J(J+1)}(\langle\hat{J}_b^2\rangle - \langle\hat{J}_c^2\rangle),$$

where the expectation values are taken with respect to the states in Eq. (9). This concludes the part of the formalism where the dimer is seen from the point of view of rigid rotor theory.

B. The quadrupole coupling in the ammonia dimer

In order to relate our six-dimensional VRT calculations to the above theory, we depart from a formula given earlier for the quadrupole splitting of E_3 and E_4 states [see Eq. (A13) of Ref. 13],

$$\langle\Phi^{\lambda}|H_{qQ}|\Phi^{\lambda}\rangle = 2\langle\psi_1^{\lambda}|q^A|\psi_1^{\lambda}\rangle \cdot \langle\theta_1^{\bar{\lambda}}|Q^A|\theta_1^{\bar{\lambda}}\rangle. \tag{15}$$

Here ψ_1^{λ} is the rovibrational part of the wave function and $\theta_1^{\bar{\lambda}}$ the nuclear spin part. In order to satisfy the Pauli principle the irreps λ and $\bar{\lambda}$ of G_{36} must be associate. Note that E_3 and E_4 are an associate pair. The factor of 2 occurs in Eq. (15) because $H_{qQ} = q^A \cdot Q^A + q^B \cdot Q^B$ and the second term has the same expectation value as the first term. Recall in this connection that the E_i states describe two interacting *para* mo-

ecules. In the notation of Eq. (15) the space-fixed magnetic quantum numbers (the projections of the angular momenta on the space-fixed Z axis) are suppressed. According to the discussion following Eq. (A13) in Ref. 13, we must diagonalize a $(2J+1)N \times (2J+1)N$-dimensional first-order matrix. Here N is the spin statistical weight, as for instance given in Table VII of Ref. 13.

Couple the *para* proton spin ($S_A = S_B = 1/2$) functions of A and B:

$$|SM_S\rangle = \sum_{m_A m_B} |\tfrac{1}{2}, m_A\rangle |\tfrac{1}{2}, m_B\rangle \langle \tfrac{1}{2}, m_A; \tfrac{1}{2}, m_B | SM_S\rangle, \quad S = 0, 1.$$

(16)

From the permutation property of Clebsch–Gordan coefficients,

$$\langle j_1 m_1; j_2 m_2 | JM\rangle = (-1)^{j_1 + j_2 - J} \langle j_2 m_2; j_1 m_1 | JM\rangle \quad (17)$$

follows that the interchange operator $\hat{I}^{ag} = (14)(25)(36)(78)$ (1, 2, 3 and 4, 5, 6 are the protons of A and B, respectively; 7 and 8 designate the nitrogens) acts as

$$\hat{I}^{ag} |SM_S\rangle |\mathcal{T}M_{\mathcal{T}}\rangle = (-1)^{S + \mathcal{T} + 1} |SM_S\rangle |\mathcal{T}M_{\mathcal{T}}\rangle. \quad (18)$$

The E_3 ($\epsilon_{\tilde{\lambda}} = 1$) and the E_4 ($\epsilon_{\tilde{\lambda}} = -1$) spin kets are

$$\theta_1^{\lambda} \equiv \tfrac{1}{2}(\hat{E} + \epsilon_{\tilde{\lambda}} \hat{I}^{ag}) |SM_S\rangle |\mathcal{T}M_{\mathcal{T}}\rangle$$

$$= \tfrac{1}{2}(1 + \epsilon_{\tilde{\lambda}}(-1)^{S + \mathcal{T} + 1}) |SM_S\rangle |\mathcal{T}M_{\mathcal{T}}\rangle. \quad (19)$$

Hence the 21 E_3 spin functions are: $\{|1M_S\rangle|00\rangle\}$, $\{|1M_S\rangle|2M_{\mathcal{T}}\rangle\}$, and $\{|00\rangle|1M_{\mathcal{T}}\rangle\}$. The 15 E_4 spin functions are: $|00\rangle|00\rangle$, $\{|00\rangle|2M_{\mathcal{T}}\rangle\}$, and $\{|1M_S\rangle|1M_{\mathcal{T}}\rangle\}$, where M_S and $M_{\mathcal{T}}$ run over the appropriate ranges.

Reintroducing the space-fixed magnetic quantum numbers, we find that we must diagonalize a matrix with general element ($\lambda = E_3, E_4$ and $\tilde{\lambda} = E_4, E_3$, respectively),

$$\langle \lambda J M_J' S' M_S' \mathcal{T}' M_{\mathcal{T}}' | 2q^A \cdot Q^A | \lambda J M_J S M_S \mathcal{T} M_{\mathcal{T}}\rangle. \quad (20)$$

Define the $(2J+1) \times (2J+1)$ field gradient matrix

$$G_{-\mu}^{(\lambda)} = (\langle \lambda J M_J' | q_{-\mu}^A | \lambda J M_J\rangle)$$

and the $(2\mathcal{T}'+1) \times (2\mathcal{T}+1)$ nuclear quadrupole matrix

$$Q_{\mu}^{\mathcal{T}', \mathcal{T}} = (\langle \mathcal{T}' M_{\mathcal{T}}' | Q_{\mu}^A | \mathcal{T} M_{\mathcal{T}}\rangle),$$

then the $\lambda = E_3$ matrix of Eq. (20) factorizes into a proton, nitrogen, and spatial factor

$$2 \sum_{\mu} (-1)^{\mu} \left[\begin{pmatrix} \langle 11|11\rangle & 0 & 0 \\ 0 & \langle 10|10\rangle & 0 \\ 0 & 0 & \langle 1-1|1-1\rangle \end{pmatrix} \otimes Q_{\mu}^{1,1} \right.$$

$$\left. \oplus \langle 00|00\rangle \otimes \begin{pmatrix} Q_{\mu}^{0,0} & Q_{\mu}^{0,2} \\ Q_{\mu}^{2,0} & Q_{\mu}^{2,2} \end{pmatrix} \right] \otimes G_{-\mu}^{(E_3)}.$$

And also the $\lambda = E_4$ matrix

$$2 \sum_{\mu} (-1)^{\mu} \left[\begin{pmatrix} \langle 11|11\rangle & 0 & 0 \\ 0 & \langle 10|10\rangle & 0 \\ 0 & 0 & \langle 1-1|1-1\rangle \end{pmatrix} \right.$$

$$\left. \otimes \begin{pmatrix} Q_{\mu}^{0,0} & Q_{\mu}^{0,2} \\ Q_{\mu}^{2,0} & Q_{\mu}^{2,2} \end{pmatrix} \oplus \langle 00|00\rangle \otimes Q_{\mu}^{1,1} \right] \otimes G_{-\mu}^{(E_4)}.$$

Since the proton spin matrices are unit matrices, we must diagonalize the two matrices

$$2 \sum_{\mu} (-1)^{\mu} Q_{\mu}^{1,1} \otimes G_{-\mu}^{(\lambda)}$$

and

$$2 \sum_{\mu} (-1)^{\mu} \begin{pmatrix} Q_{\mu}^{0,0} & Q_{\mu}^{0,2} \\ Q_{\mu}^{2,0} & Q_{\mu}^{2,2} \end{pmatrix} \otimes G_{-\mu}^{(\lambda)}.$$

These matrices may be block-diagonalized by Clebsch–Gordan coupling the basis $|JM_J\rangle|\mathcal{T}M_{\mathcal{T}}\rangle$ to $|(J\mathcal{T})FM_F\rangle$ for arbitrary $\mathcal{T}', \mathcal{T} = 0, 1, 2$. We proceed in the very same way as in the derivation of Eq. (4), and find

$$H_{\mathcal{T}'\mathcal{T}} = 2\langle \lambda, (J\mathcal{T}')FM_F | q^A \cdot Q^A | \lambda, (J\mathcal{T})FM_F\rangle$$

$$= 2(-1)^{\mathcal{T}_1} \langle \lambda, J || q^A || \lambda, J\rangle \langle I_A || Q^A || I_A\rangle [(2\mathcal{T}+1)$$

$$\times (2\mathcal{T}'+1)]^{1/2} \begin{Bmatrix} F & \mathcal{T}' & J \\ 2 & J & \mathcal{T} \end{Bmatrix} \begin{Bmatrix} I_A & \mathcal{T}' & I_B \\ \mathcal{T} & I_A & 2 \end{Bmatrix}. \quad (21)$$

The reduced matrix elements are defined as in Eq. (5). We will show that the matrix element

$$\langle \lambda, J, J | q_0^A | \lambda, J, J\rangle \equiv \langle \psi_1^{\lambda} | q_0^A | \psi_1^{\lambda}\rangle \quad (22)$$

of the field gradient operator can be identified with q_J. In order to evaluate it, we assume that the field gradient q^X at nucleus N_X is the same as in the free monomer X. From the axial symmetry of the ammonia monomer then follows that only one component $q \equiv q_0^{NH_3}$ must be considered in the monomer frame. If we successively transform from the monomer- to the dimer- to the space-fixed frame we obtain

$$q_{\mu}^A = q_0^{NH_3} \sum_{\nu} D_{\mu\nu}^{(2)}(\alpha, \beta, 0)^* D_{\nu 0}^{(2)}(\gamma_A, \vartheta_A, \varphi_A)^*$$

$$= q_0^{NH_3} \sum_{\nu} D_{\mu\nu}^{(2)}(\alpha, \beta, 0)^* C_{\nu}^{(2)}(\vartheta_A, \gamma_A)$$

$$= \sum_{\nu} D_{\mu\nu}^{(2)}(\alpha, \beta, \gamma)^* (q_0^{NH_3} C_{\nu}^{(2)}(\vartheta_A, \tfrac{1}{2}\bar{\gamma})). \quad (23)$$

Integration over the internal wave function and comparison with Eq. (2) will give us an expression for the dimer-fixed field gradient tensor $\bar{q}^X$. We use that the E_3 and E_4 states ψ_1^{λ} in Eq. (22) are

$$|\psi_1^{\lambda}\rangle = \frac{1}{\sqrt{2}}(\hat{E} + \epsilon_{\lambda} \hat{I}^{ag}) |J, K\rangle |\lambda, K\rangle, \quad (24)$$

with $\epsilon_\lambda = +1$ for $\lambda = E_3$ and $\epsilon_\lambda = -1$ for $\lambda = E_4$. See Ref. 13 for the derivation of this result, but note that Ω, instead of K was used in that reference. The weak dependence of the "internal" wave functions $|\lambda,K\rangle$ on J is neglected and $K(=1)$ is fixed if we neglect the Coriolis coupling. The "external" functions are

$$|J,K\rangle = \left(\frac{2J+1}{4\pi}\right)^{1/2} D_{JK}^{(J)}(\alpha,\beta,0)^*. \tag{25}$$

These functions differ from the symmetric top functions of Eq. (10) by a factor $(2\pi)^{-1/2} \exp(iK\gamma)$, but it can easily be shown that the external factors in the matrix elements below are identical to the usual rigid rotor expressions used in Sec. II A. The internal functions are the VRT states

$$|\lambda,K\rangle = \sum_i c_{iK}^\lambda |j_{A_i},k_{A_i},j_{B_i},k_{B_i},j_i,K,n_i\rangle \tag{26}$$

with the basis defined as in Refs. 13 and 19:

$$|j_A,k_A,j_B,k_B,j,K,n\rangle$$

$$= \chi_n(R) \sum_{m_A m_B} D_{m_A k_A}^{(j_A)}(\gamma_A,\vartheta_A,\varphi_A)^*$$

$$\times D_{m_B k_B}^{(j_B)}(\gamma_B,\vartheta_B,\varphi_B)^* \langle j_A m_A; j_B m_B|jK\rangle.$$

The interchange operator $\hat{I}^{ag}$ acts as follows on these functions:

$$\hat{I}^{ag}|J,K\rangle = (-1)^J |J,-K\rangle, \tag{27a}$$

$$\hat{I}^{ag}|\lambda,K\rangle = \sum_i c_{iK}^\lambda (-1)^{j_{A_i}+j_{B_i}} |j_{B_i},k_{B_i},j_{A_i},k_{A_i},j_i,-K,n_i\rangle. \tag{27b}$$

Since $\hat{I}^{ag}|\lambda,K\rangle$ does not interact with $|\lambda,K\rangle$ for $K \neq 0$, when we neglect the off-diagonal Coriolis coupling, the coefficients $c_{iK}^{E_3}$ and $c_{iK}^{E_4}$ are equal. Substitution of Eqs. (24)–(27) into (22) yields

$$\langle\psi_1^\lambda|q_0^A|\psi_1^\lambda\rangle = \tfrac{1}{2}q_0^{NH_3}[\langle J,K|C_0^{(2)}(\beta,0)|J,K\rangle\langle\lambda,K|C_0^{(2)}(\vartheta_A,\gamma_A)|\lambda,K\rangle + \langle J,-K|C_0^{(2)}(\beta,0)|J,-K\rangle$$

$$\times \langle\lambda,K|\hat{I}^{ag}C_0^{(2)}(\vartheta_A,\gamma_A)\hat{I}^{ag}|\lambda,K\rangle + \epsilon_\lambda(-1)^J\langle J,K|C_2^{(2)}(\beta,0)|J,-K\rangle\langle\lambda,K|C_2^{(2)}(\vartheta_A,\gamma_A)\hat{I}^{ag}|\lambda,K\rangle$$

$$+ \epsilon_\lambda(-1)^J\langle J,-K|C_{-2}^{(2)}(\beta,0)|J,K\rangle\langle\lambda,K|\hat{I}^{ag}C_{-2}^{(2)}(\vartheta_A,\gamma_A)|\lambda,K\rangle]. \tag{28}$$

Using the pairwise equality of the rotational matrix elements, we find

$$\langle\psi_1^\lambda|q_0^A|\psi_1^\lambda\rangle$$

$$= \tfrac{1}{2}q_0^{NH_3}[\langle J,K|C_0^{(2)}|J,K\rangle\langle\lambda,K| C_0^{(2)}(\vartheta_A,\gamma_A)$$

$$+ \hat{I}^{ag}C_0^{(2)}(\vartheta_A,\gamma_A)\hat{I}^{ag}|\lambda,K\rangle + \epsilon_\lambda(-1)^J$$

$$\times \langle J,K|C_2^{(2)}|J,-K\rangle\langle\lambda,K|C_2^{(2)}(\vartheta_A,\gamma_A)\hat{I}^{ag} + \hat{I}^{ag}C_{-2}^{(2)}$$

$$\times(\vartheta_A,\gamma_A)|\lambda,K\rangle]. \tag{29}$$

One may show that $\hat{I}^{ag}C_\nu^{(2)}(\vartheta_A,\gamma_A)\hat{I}^{ag} = C_{-\nu}^{(2)}(\vartheta_B,\gamma_B)$. Using this, we find

$$\langle\psi_1^\lambda|q_0^A|\psi_1^\lambda\rangle = \tfrac{1}{2}q_0^{NH_3}[\langle J,K|C_0^{(2)}|J,K\rangle\langle\lambda,K |C_0^{(2)}(\vartheta_A,\gamma_A)$$

$$+ C_0^{(2)}(\vartheta_B,\gamma_B)|\lambda,K\rangle + \epsilon_\lambda(-1)^J$$

$$\times \langle J,K|C_2^{(2)}|J,-K\rangle\langle\lambda,K| [C_2^{(2)}(\vartheta_A,\gamma_A)$$

$$+ C_2^{(2)}(\vartheta_B,\gamma_B)]\hat{I}^{ag}|\lambda,K\rangle]. \tag{30}$$

Finally we may substitute $\langle\psi_1^\lambda|q_0^A|\psi_1^\lambda\rangle$ with $q_0^{NH_3}\equiv q$ and $\langle I_A,I_A|Q_0^A|I_A,I_A\rangle = eQ$ into Eqs. (21) and (22). We now observe that our result (30) has the same form as the rigid rotor result, Eq. (12), and that indeed q_J may be identified with $\langle\psi_1^\lambda|q_0^A|\psi_1^\lambda\rangle$. The coupling constants χ_{gg} in the rigid rotor formula can be expressed in terms of matrix elements over the internal wave functions, i.e., the VRT states, as follows:

$$\chi_{aa} = \tfrac{1}{2}eQq\langle\lambda,K|C_0^{(2)}(\vartheta_A,\gamma_A) + C_0^{(2)}(\vartheta_B,\gamma_B)|\lambda,K\rangle,$$

$$\chi_{bb}-\chi_{cc} = \tfrac{1}{2}\sqrt{6}eQq\langle\lambda,K|[C_2^{(2)}(\vartheta_A,\gamma_A)$$

$$+ C_2^{(2)}(\vartheta_B,\gamma_B)]\hat{I}^{ag}|\lambda,K\rangle \tag{31}$$

with the free monomer value $eQq = -4.08983$ MHz.[23] Comparing Eqs. (30) and (12), we see that the parities of the E_3 and E_4 states in $(NH_3)_2$ are related to the parities of the rigid rotor states as

$$\epsilon_\lambda \leftrightarrow (-1)^{K_a+K_c}. \tag{32}$$

Recalling that we are considering the prolate symmetric top case $K \equiv K_a = 1$, it follows that the rigid rotor states with *odd* K_c must correspond with the E_3 states and those with *even* K_c with the E_4 states.

Although the quadrupole splittings can be computed as if the dimer were a rigid prolate top—which in reality it is not—the selection rules do not agree. In Ref. 13 it is shown by invoking G_{36} symmetry that the dipole transitions are of the type $E_3 \rightarrow E_3$ and $E_4 \rightarrow E_4$, i.e., $\Delta\epsilon_\lambda = 0$. On the other hand, the selection rule for the prolate top with the wave function of Eq. (9) and a dipole μ_a along the a axis, is $\Delta K_a = 0$ and $\Delta K_c = 1$ (see Ref. 21, p. 255), which by Eq. (32) does not apply to the ammonia dimer. The perpendicular μ_b and μ_c transitions require $\Delta K_a = 1$, and do not have to be considered further, since we have only observed $\Delta K_a = 0$ transitions.
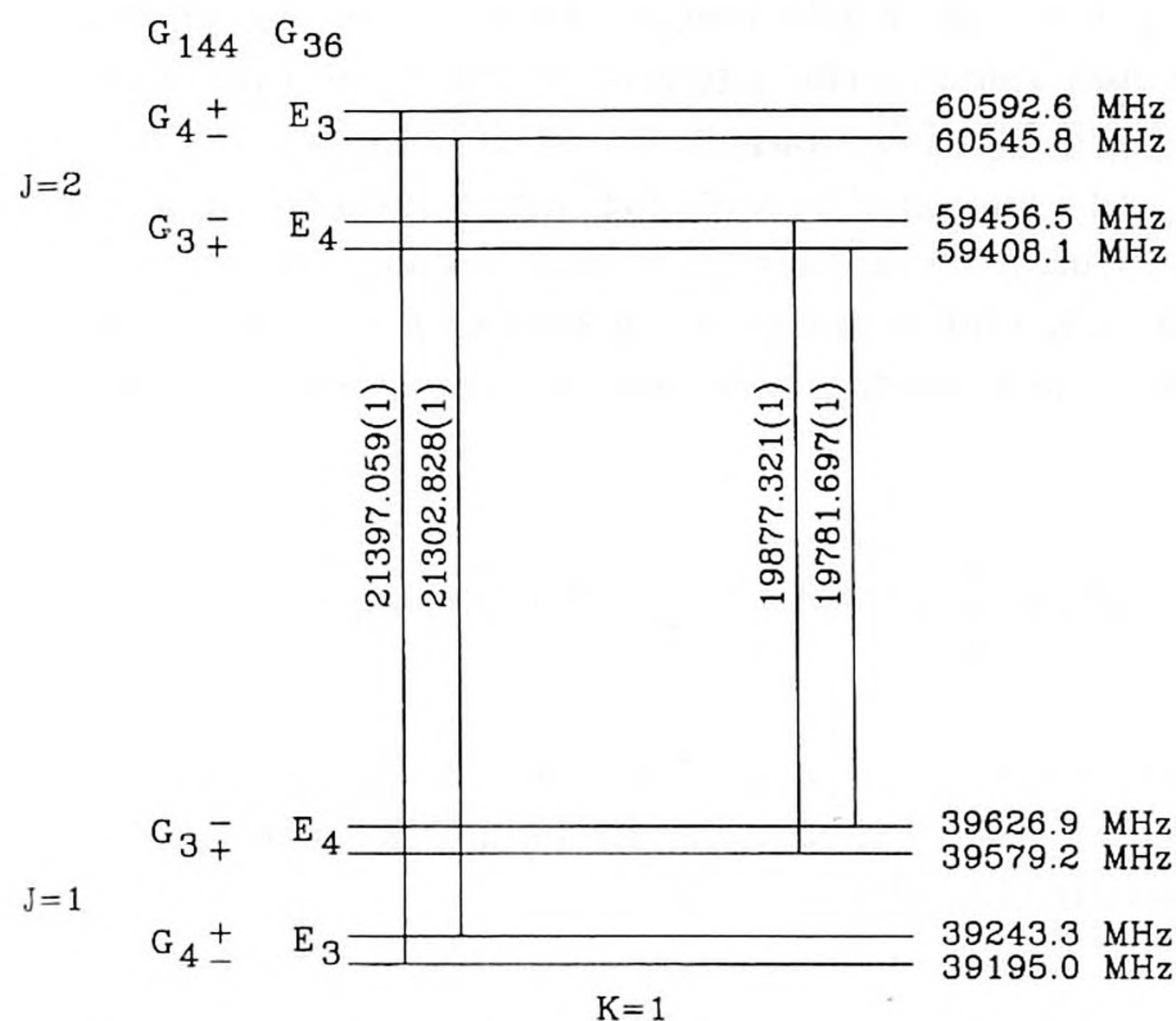
FIG. 1. Lowest E_3 and E_4 levels with $|K|=1$ and $J=1,2$ from Loeser *et al.*, Ref. 12. The E_3-E_4 splitting is only caused by Coriolis mixing, see Ref. 19, and the further splitting into $G_4^\pm$ and $G_3^\pm$ doublets is due to hindered umbrella inversion, see Ref. 20. The vertical lines indicate the dipole allowed rotational transitions observed in this experiment, with the frequencies from the fit in Table V.

Note finally that we obtain the rigid rotor expression only by neglecting the off-diagonal Coriolis coupling, which mixes states of different $|K|$. In Ref. 19 this coupling has been explicitly included in the calculation of the VRT states. In Sec. IV we will show to what extent it affects the calculated hyperfine coupling constants.

III. EXPERIMENT

All experiments were carried out using the pulsed molecular beam (MB) Fourier transform microwave (FTMW) spectrometer of the Kiel microwave group. Technical details are given in Ref. 24. The apparatus was operated in its high resolution mode pulsing the molecular beam through one of the mirrors.[25] Under these conditions a minimum linewidth of approximately 2 kHz at 12 GHz can be achieved. All lines are split into doublets separated by twice the Doppler shift according to the velocity of the molecular beam. The transition frequencies were obtained as the arithmetic mean of the Doppler components. The spectra were taken using a sample containing 1% ammonia in helium at a stagnation pressure of 100 kPa. Since the approximate line positions could easily be derived from the energy levels given in Ref. 12, see Fig. 1, the hyperfine patterns were found immediately. Because the hyperfine components were spread over a range of approximately 4 MHz, several measurements at different polarizing frequencies were necessary to cover the whole pattern. Each spectrum shown in Figs. 2 and 3 is therefore composed of four spectra polarized at different frequencies. The amplitudes are roughly adjusted for a constant signal-to-noise ratio in the whole range. The observed frequencies are compiled in Table I.
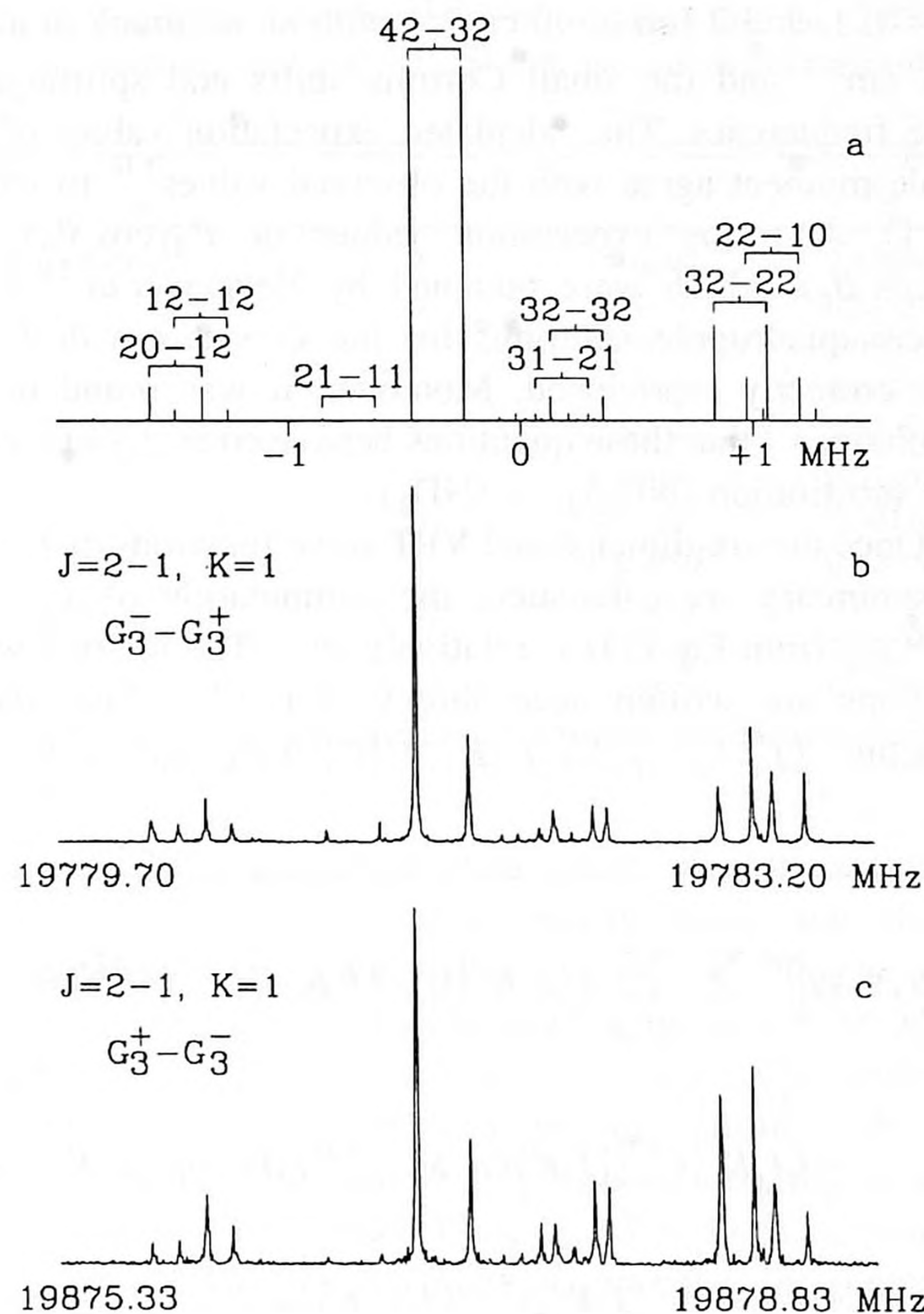

FIG. 2. $J=2-1$, $|K|=1$, E_4-E_4 transitions. (a) Theoretical spectrum: Doppler doublets marked by brackets, quantum numbers F and $\mathscr{T}$ in the $(I_A,I_B)\mathscr{T},J,F$ coupling scheme used, intensities corrected for nuclear spin statistics; (b) $G_3^- - G_3^+$ transitions; (c) $G_3^+ - G_3^-$ transitions. Recording conditions: Sample: 1% ammonia in helium, polarizing pulses: 1 mW, 100 ns, Fourier transform: 4096 data points, averaging cycles: 4096.

IV. RESULTS

A. Calculated

First we present the results calculated with and without Coriolis coupling. The six-dimensional wave functions of the lowest E_3 and E_4 states were obtained by solving the Schrödinger equation in a symmetry adapted basis of coupled free rotor functions and radial basis functions, cf. Eqs. (24)–(26). This has been described extensively in Refs. 13, 19, and 26. The maximum j_A and j_B value of the internal rotor basis was 7. Three radial basis functions were used. These were obtained by solving a one-dimensional radial Schrödinger equation, with the Hamiltonian consisting of the radial kinetic energy and the R-dependent potential with the monomer orientations fixed at the equilibrium angles. In Ref. 19 the potential was modeled by adding the electrostatic interactions between the dipole, quadrupole, and octupole moments of the ammonia monomers to an exp-6 atom–atom potential which represents the exchange repulsion and dispersion interactions. The pre-exponential factors in the terms which model the repulsion were optimized, in such a manner that the splittings between the energy levels of the lowest VRT states with $K=0$ agree with the far-infrared frequencies measured by Loeser *et al.*[12] These splittings are caused by interchange tunneling. The resulting potential was able to reproduce all the observed far-infrared frequencies for

$|K| = 0$, 1, and 2 (up to 40 cm^{-1}) with an accuracy of about 0.25 cm^{-1} and the small Coriolis shifts and splittings of these frequencies. The calculated expectation values of the dipole moment agree with the observed values[7,14] to within 0.1 D. Also the expectation values of $P_2(\cos \vartheta_A)$ and $P_2(\cos \vartheta_B)$, which were obtained by Nelson *et al.*[7,8] from nuclear quadrupole splittings for the G states with $K=0$, were correctly reproduced. Moreover, it was found in the calculations[19] that these quantities behave correctly upon isotope substitution $(NH_3)_2 \rightarrow (ND_3)_2$.

Once the six-dimensional VRT wave functions of E_3 and E_4 symmetry are calculated, the computation of χ_{aa} and $\chi_{bb} - \chi_{cc}$ from Eq. (31) is relatively easy. The internal wave functions are written according to Eq. (26). The matrix elements $\langle j'_A, k'_A, j'_B, k'_B, j', K', n' | C^{(2)}_\nu(\vartheta_X, \gamma_X) | j_A, k_A, j_B,$

$k_B, j, K, n \rangle$ are easily determined by standard angular momentum algebra. The action of $\hat{I}^{ag}$ on a primitive function is given in Eq. (27b) and causes no difficulties.

As mentioned before, the above formulas apply to the case where Coriolis coupling is neglected, i.e., when $|K|$ is a good quantum number. If we take Coriolis mixing into account, the wave function contains components with different $|K|$:

$$|\psi_1^\lambda\rangle = \frac{1}{\sqrt{2}}(\hat{E} + \epsilon_\lambda \hat{I}^{ag}) \sum_K |J,K\rangle |\lambda,K\rangle, \tag{33}$$

where the internal wave functions $|\lambda,K\rangle$ are defined as in Eq. (26). The next steps are trivial and we arrive at a simple generalization of Eq. (30):

$$q_J = \tfrac{1}{2}q_0^{NH_3} \sum_\nu \sum_{K',K} [\langle J,K'|C^{(2)}_\nu|J,K\rangle\langle\lambda,K'|C^{(2)}_\nu(\vartheta_A,\gamma_A)|\lambda,K\rangle$$

$$+ \langle J,K'|C^{(2)}_{-\nu}|J,K\rangle\langle\lambda,K'|C^{(2)}_{-\nu}(\vartheta_B,\gamma_B)|\lambda,K\rangle + \epsilon_\lambda(-1)^J\langle J,K'|C^{(2)}_\nu|J,-K\rangle\langle\lambda,K' \mid C^{(2)}_\nu(\vartheta_A,\gamma_A)\hat{I}^{ag}|\lambda,K\rangle$$

$$+ \epsilon_\lambda(-1)^J\langle J,K'|C^{(2)}_{-\nu}|J,-K\rangle\langle\lambda,K' \mid C^{(2)}_{-\nu}(\vartheta_B,\gamma_B)\hat{I}^{ag}|\lambda,K\rangle]. \tag{34}$$

In Table II we show the different contributions in this expression for the lowest E_3 and E_4 states with $J=1$ and, mainly, $|K|=1$. The values without Coriolis coupling are obtained by inserting into Eq. (34) the eigenvectors calculated with purely $|K|=1$ basis functions or, equivalently, by the use of Eq. (30). The $\nu = \pm 1$ contributions are zero, of course. Inserting into Eq. (34) a Coriolis mixed eigenvector of mainly $|K|=1$ character, but with some admixture of $K=0$ components, we obtain the other values in Table II. The $\nu = \pm 1$ contributions arise from the off-diagonal matrix elements between the $|K|=1$ and $K=0$ components. For the E_3 state these contributions are very small, for the E_4 state they are larger. This is due to the strong Coriolis perturbation of the latter state by the $J=1$, $K=0$ state of E_4 symmetry which lies only 0.97 cm^{-1} lower, see Ref. 12. It is this perturbation which actually causes the splitting between these E_3 and E_4 levels.[19] The contributions for $\nu=0$ and $\nu=\pm2$ are just slightly changed by the Coriolis mixing, for both the E_3 and E_4 states. In the rigid rotor case these are the only nonvanishing contributions, and it is from these terms that we extract the quadrupole coupling constants χ_{aa} and $\chi_{bb}-\chi_{cc}$, by the use of Eq. (31). The fact that the $\nu=\pm1$ contributions for the E_4 state are not negligible implies, however, that the fit of the observed hyperfine splittings by the rigid rotor formulas in Sec. II A will not be perfect. From the calculations for $J=1$ with the pure $|K|=1$ states of E_3 and E_4 symmetry we find, through Eq. (31), that $\chi_{aa}=0.1179$ MHz and $\chi_{bb}-\chi_{cc}=1.9595$ MHz.

Before we describe the measured results, one more observation has to be made in order to understand the spectra.
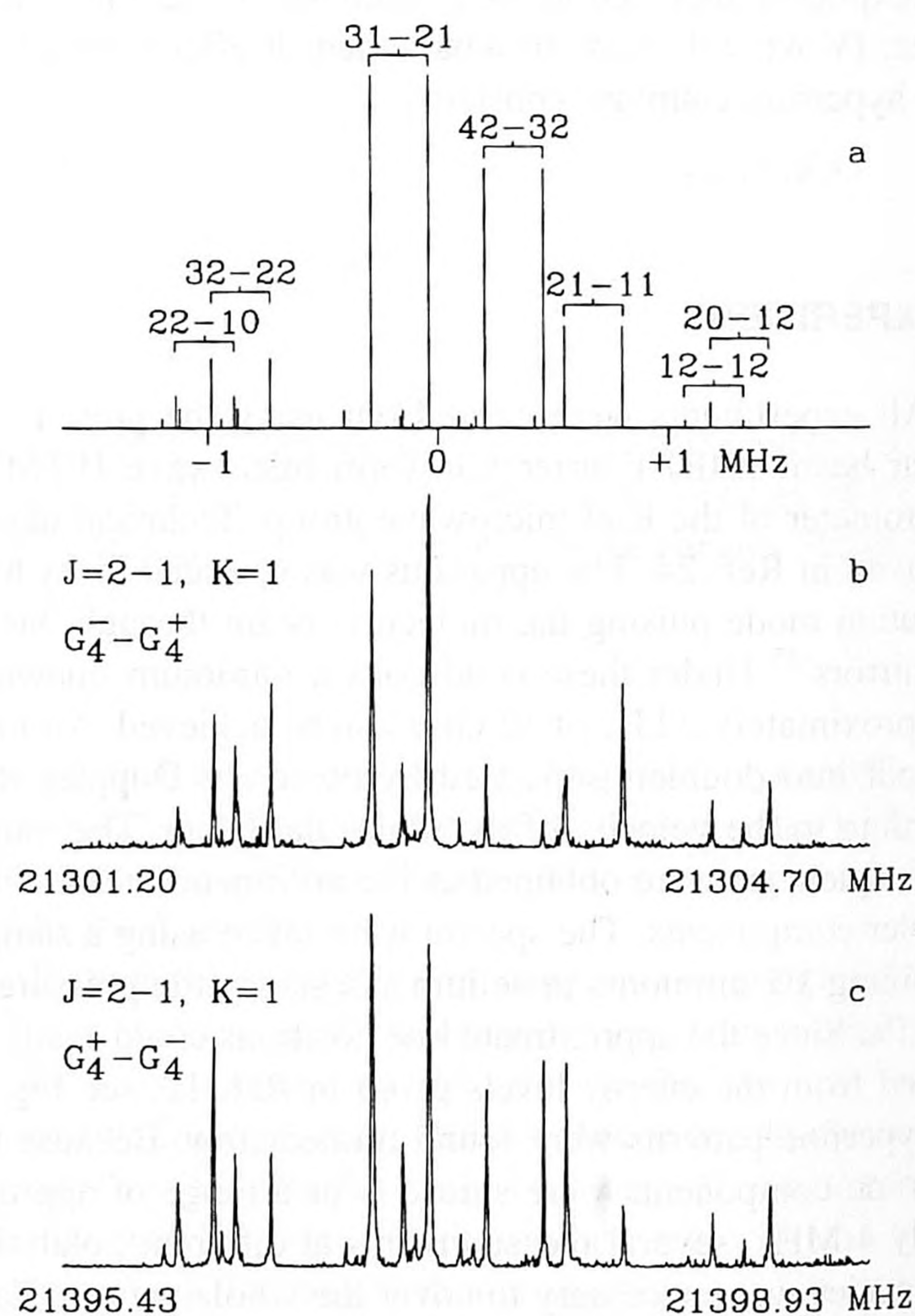

FIG. 3. $J=2-1$, $|K|=1$, E_3-E_3 transitions. (a) Theoretical spectrum, (b) $G_4^- - G_4^+$ transitions, (c) $G_4^+ - G_4^-$ transitions. For recording conditions se Fig. 2.

TABLE I. Observed transitions of $(NH_3)_2$ and their fit in terms of the rigid rotor coupling constants χ_{aa} and $\chi_{bb}-\chi_{cc}$. F and $\mathscr{I}$ are the total and intermediate angular momentum quantum numbers in the coupling scheme $(I_A,I_B)\mathscr{I},J,F$. ν_0 designates the hyperfine free line centers, ν the observed hyperfine components, $\Delta\nu_{obs}$ (MHz) the observed splittings with respect to ν_0, $\Delta\nu_{calc}$ (MHz) the splitting calculated from the fitted quadrupole coupling constants, and δ the observed-minus-calculated values (kHz).

$2_{11}-1_{11}$, $G_4^+ - G_4^-$, $\nu_0 = 21397.049(5)$ MHz

$F''\mathscr{I}'' - F\mathscr{I}$	ν	$\Delta\nu_{obs}$	$\Delta\nu_{calc}$	δ
2 0–1 2	21398.367	1.318	1.321	−3
1 2–1 2	21398.253	1.204	1.216	−12
2 1–1 1	21397.736	0.686	0.671	15
4 2–3 2	21397.390	0.340	0.326	14
3 1–2 1	21396.891	−0.159	−0.163	4
3 2–3 2	21396.778	−0.272	−0.249	−23
3 2–2 2	21396.207	−0.843	−0.854	11
2 2–1 0	21396.051	−0.998	−0.994	−4
2 2–2 2	21395.993	−1.057	−1.055	−2

$2_{11}-1_{11}$, $G_4^- - G_4^+$, $\nu_0 = 21302.824(6)$ MHz

$F''\mathscr{I}'' - F\mathscr{I}$	ν	$\Delta\nu_{obs}$	$\Delta\nu_{calc}$	δ
2 0–1 2	21304.135	1.311	1.321	−9
2 1–1 1	21303.504	0.680	0.671	8
4 2–3 2	21303.157	0.333	0.326	7
3 1–2 1	21302.660	−0.164	−0.163	−1
3 2–2 2	21301.975	−0.849	−0.854	5
2 2–1 0	21301.820	−1.004	−0.994	−10

$2_{12}-1_{10}$, $G_3^+ - G_3^-$, $\nu_0 = 19877.309(5)$ MHz

$F''\mathscr{I}'' - F\mathscr{I}$	ν	$\Delta\nu_{obs}$	$\Delta\nu_{calc}$	δ
2 2–1 0	19878.408	1.099	1.106	−8
3 2–2 2	19878.268	0.958	0.950	9
3 2–3 2	19877.560	0.250	0.277	−27
3 1–2 1	19877.498	0.189	0.181	7
4 2–3 2	19876.964	−0.345	−0.363	17
2 1–1 1	19876.583	−0.727	−0.747	20
1 2–1 2	19875.947	−1.363	−1.352	−11
2 0–1 2	19875.832	−1.477	−1.469	−8

$2_{12}-1_{10}$, $G_3^- - G_3^+$, $\nu_0 = 19781.685(5)$ MHz

$F''\mathscr{I}'' - F\mathscr{I}$	ν	$\Delta\nu_{obs}$	$\Delta\nu_{calc}$	δ
2 2–1 0	19782.784	1.099	1.106	−7
3 2–2 2	19782.643	0.958	0.950	8
3 2–3 2	19781.937	0.251	0.277	−26
3 1–2 1	19781.876	0.190	0.181	9
4 2–3 2	19781.339	−0.346	−0.363	17
2 1–1 1	19780.958	−0.728	−0.747	19
1 2–1 2	19780.322	−1.364	−1.352	−11
2 0–1 2	19780.208	−1.477	−1.469	−8

The irreducible representations E_3 and E_4 pertain to the symmetry group G_{36} of the ammonia dimer with rigid monomers. In reality, the NH_3 monomers are still umbrella-inverting, although much slower than in the free monomer; the resulting tunneling splittings have been measured by Loeser *et al.*[12] It has been explained by Olthof *et al.*[20] why the hindered umbrella inversions cause splittings of the different VRT states which vary over three orders of magnitude. Each E_3 level splits into a $G_4^\pm$ doublet and each E_4 level into a $G_3^\pm$ doublet. The latter irreducible representations belong to G_{144}, the symmetry group of the dimer with inverting

TABLE II. Contributions to eQq_J (in MHz) calculated from Eq. (34) without Coriolis coupling, for $J=|K|=1$, and with the Coriolis mixing involving $K=0$.

	ν	E_3	E_4
Without Coriolis	−2	−0.10594	0.10594
	0	0.01156	0.01156
	2	−0.09001	0.09001
	total	−0.18439	0.20751
With Coriolis	−2	−0.10594	0.10466
	−1	−0.00097	0.02656
	0	0.01178	0.00110
	1	−0.00080	0.02094
	2	−0.09001	0.08893
	total	−0.18594	0.25207
Experimental	total	−0.2562	0.3142

monomers. Both experiment[12] and theory[20] find the splittings of the E_3 and E_4 levels to be nearly equal, and almost J-independent. For the lowest E_3 and E_4 levels with $|K|=1$ this splitting was measured[12] to be about 48 MHz; the calculations[20] agree well with this value. The umbrella inversion has no effect on the hyperfine splittings: the $G_4^\pm$ and $G_3^\pm$ doublets are split by the nuclear quadrupole coupling by equal amounts, see Table I, and in the same manner as the E_3 and E_4 levels. The selection rules for rotational transitions are: $E_3 \leftrightarrow E_3$ and $E_4 \leftrightarrow E_4$ in G_{36} symmetry, and $G_4^+ \leftrightarrow G_4^-$ and $G_3^+ \leftrightarrow G_3^-$ in G_{144} symmetry.

B. Measured

As noted above, a rigid rotor program was used for the analysis of the experimental nitrogen hyperfine splittings in the ammonia dimer. The values of D_1 and D_2 for the asymmetric rotor states used in our analysis, cf. Eq. (14), are listed in Table III. In order to mimic a prolate symmetric top, we introduced into our asymmetric rotor program an arbitrarily large rotational constant $A=10^4$ GHz. As derived at the end of Sec. II B, the selection rules for the $\Delta|K|=0$ transitions $E_3 \leftrightarrow E_3$ and $E_4 \leftrightarrow E_4$ in $(NH_3)_2$ are just opposite to the selection rules for transitions between the corresponding rigid rotor states. Hence, in our rigid rotor fitting program we had to introduce the selection rule $\Delta K_c=0$, rather than the usual rule $|\Delta K_c|=1$ for parallel transitions. Using a least squares fitting routine the hyperfine free line centers ν_0 and the quadrupole coupling constants χ_{aa} and $\chi_{bb}-\chi_{cc}$ were fitted to the experimental data given in Table I. All four observed transitions were fitted simultaneously yielding the coupling constants $\chi_{aa}=0.1509(83)$ MHz and $\chi_{bb}-\chi_{cc}=2.8365(83)$

TABLE III. Expectation values of the squared angular momenta in the asymmetric rotor basis of Eq. (9). Column 1 gives the symmetry species λ under G_{36}, column 2 the corresponding asymmetric rotor quantum numbers. The D_1 and D_2 constants are defined in Eq. (14).

λ	$J_{K_a K_c}$	$\langle J_a^2 \rangle$	$\langle J_b^2 \rangle$	$\langle J_c^2 \rangle$	D_1	D_2
E_3	1_{11}	1	0	1	1/2	−1/2
E_3	2_{11}	1	4	1	−1/2	1/2
E_4	1_{10}	1	1	0	1/2	1/2
E_4	2_{12}	1	1	4	−1/2	−1/2

TABLE IV. Values of eQq_J (in MHz) obtained from fitting the measured $E_3 \leftrightarrow E_3$ ($G_4^\pm \leftrightarrow G_4^\mp$) and $E_4 \leftrightarrow E_4$ ($G_3^\pm \leftrightarrow G_3^\mp$) transitions. In parentheses: the standard errors in the fit.

	$J=1$	$J=2$
E_3 (separate fit)	−0.2562 (7)	0.4060(13)
(global fit)	−0.2686(12)	0.3837(16)
E_4 (separate fit)	0.3142 (6)	−0.3977(11)
(global fit)	0.2987(15)	−0.4268(21)

MHz. It is found, as expected from the presence of the non-vanishing terms with $\nu = \pm 1$ (see Sec. IV A), that the error in the fit (≈ 8 kHz) is somewhat larger than the error (of ≈ 1 kHz) which usually occurs for nearly rigid rotor systems.

In order to avoid this fitting error, we have also fitted the measured hyperfine splittings in terms of the quantity eQq_J, which is defined exactly for the E_3 and E_4 states of the ammonia dimer by Eq. (34). Four values of this quantity are relevant here, because eQq_J is different for the E_3 and E_4 states and different for $J=1$ and $J=2$. These four parameters can be fitted simultaneously to all the observed transition frequencies or they can be fitted separately for the $E_3 \leftrightarrow E_3$ and $E_4 \leftrightarrow E_4$ transitions. The resulting values are given in Table IV. From Table V it is evident that, indeed, this provides a much better fit of the observed hyperfine splittings. Although one can compare the measured values of eQq_J to those calculated with and without the Coriolis coupling, see Table II, they provide less insight in the nature of the VRT states than the parameters χ_{aa} and $\chi_{bb} - \chi_{cc}$. This is because they depend both on the internal and the external (i.e., overall rotational) part of the wave functions, cf. Eqs. (30) and (34), whereas the latter parameters depend only on the internal part, cf. Eq. (31). Rather than to obtain χ_{aa} and $\chi_{bb} - \chi_{cc}$ from a direct fit to the experimental data, it is also possible to compute them from the fitted values of eQq_J in Table IV, with the use of Eq. (13) and the values of D_1 and D_2 from Table III. This cannot be done for the $E_3 \leftrightarrow E_3$ and $E_4 \leftrightarrow E_4$ transitions separately, because the equations for $J=1$ and $J=2$ are not independent. The result from the globally fitted values of eQq_J is that $\chi_{aa} = 0.1507$ MHz and $\chi_{bb} - \chi_{cc} = 2.8366$ MHz. These values are practically the same as those obtained directly from the fit of the measured frequencies.

V. DISCUSSION AND CONCLUSIONS

As is evident from Eq. (31), the quantity $\chi_{aa}/(eQq)$ with $eQq = -4.08983$ MHz is the expectation value of the Legendre polynomial $P_2(\cos \vartheta_X) = C_0^{(2)}(\vartheta_X, \gamma_X)$ averaged over the two monomers $X = A, B$. The angles ϑ_X are the angles between the monomer C_3 axes and the dimer z axis (the vector **R**). From symmetry considerations, see the Appendix of Ref. 13, it follows that only for the mixed *ortho–para* G states these quantities can be measured separately for $X = A$ and $X = B$. For all other symmetry species one measures the average quantity. Both the experimental value $[\langle P_2(\cos \vartheta_A) \rangle + \langle P_2(\cos \vartheta_B) \rangle]/2 = -0.0369$ and the calculated value -0.0288 are nearly zero, which indicates that the average of the angles ϑ_A and $180° - \vartheta_B$ is close to the

TABLE V. Observed transitions of $(NH_3)_2$ and their fit in terms of eQq_J, separately for the $G_4^\pm \leftrightarrow G_4^\mp$ and $G_3^\pm \leftrightarrow G_3^\mp$ transitions. All symbols are defined as in Table I.

$2_{11}-1_{11}$, $G_4^+ - G_4^-$, $\nu_0 = 21397.059(1)$ MHz

$F'' \mathscr{T}'' - F \mathscr{T}$	ν	$\Delta \nu_{obs}$	$\Delta \nu_{calc}$	δ
2 0−1 2	21398.367	1.308	1.306	2
1 2−1 2	21398.253	1.194	1.195	−0
2 1−1 1	21397.736	0.676	0.676	1
4 2−3 2	21397.390	0.330	0.331	−1
3 1−2 1	21396.891	−0.168	−0.166	−3
3 2−3 2	21396.778	−0.282	−0.278	−4
3 2−2 2	21396.207	−0.853	−0.854	2
2 2−1 0	21396.051	−1.008	−1.010	2
2 2−2 2	21395.993	−1.066	−1.067	1

$2_{11}-1_{11}$, $G_4^- - G_4^+$, $\nu_0 = 21302.828(1)$ MHz

$F'' \mathscr{T}'' - F \mathscr{T}$	ν	$\Delta \nu_{obs}$	$\Delta \nu_{calc}$	δ
2 0−1 2	21304.135	1.307	1.306	2
2 1−1 1	21303.504	0.676	0.676	0
4 2−3 2	21303.157	0.329	0.331	−2
3 1−2 1	21302.660	−0.168	−0.166	−2
3 2−2 2	21301.975	−0.853	−0.854	2
2 2−1 0	21301.820	−1.008	−1.010	1

$2_{12}-1_{10}$, $G_3^+ - G_3^-$, $\nu_0 = 19877.321(1)$ MHz

$F'' \mathscr{T}'' - F \mathscr{T}$	ν	$\Delta \nu_{obs}$	$\Delta \nu_{calc}$	δ
2 2−1 0	19878.408	1.087	1.085	2
3 2−2 2	19878.268	0.947	0.947	−1
3 2−3 2	19877.560	0.239	0.241	−2
3 1−2 1	19877.498	0.177	0.178	−1
4 2−3 2	19876.964	−0.357	−0.356	−1
2 1−1 1	19876.583	−0.738	−0.741	2
1 2−1 2	19875.947	−1.374	−1.377	3
2 0−1 2	19875.832	−1.488	−1.486	−2

$2_{12}-1_{10}$, $G_3^- - G_3^+$, $\nu_0 = 19781.697(1)$ MHz

$F'' \mathscr{T}'' - F \mathscr{T}$	ν	$\Delta \nu_{obs}$	$\Delta \nu_{calc}$	δ
2 2−1 0	19782.784	1.087	1.085	2
3 2−2 2	19782.643	0.946	0.947	−1
3 2−3 2	19781.937	0.240	0.241	−1
3 1−2 1	19781.876	0.179	0.178	1
4 2−3 2	19781.339	−0.358	−0.356	−2
2 1−1 1	19780.958	−0.739	−0.741	2
1 2−1 2	19780.322	−1.375	−1.377	2
2 0−1 2	19780.208	−1.489	−1.486	−3

"magic angle" of 54.7°. Experimentally we find 56.2°, our calculations yield 55.9°. This angle lies between the angles $\vartheta_A = 64.5°$ and $180° - \vartheta_B = 48.6°$ found [7,8] for the *ortho* and *para* monomers in the lowest G state. The agreement between calculations and experiment is excellent, which indicates that the semi-empirical potential of Olthof *et al.*[19] is accurate in its dependence on ϑ_A and ϑ_B. This might have been expected, since it appeared from the calculations of the VRT states[19] that the measured far-infrared spectrum[10,12] and properties[7,8,14] are mainly sensitive to the ϑ_A and ϑ_B dependence of the potential (in particular, to the height of the interchange barrier).

Although it is obvious from Eq. (31) that $\chi_{bb} - \chi_{cc}$ will contain information about the dihedral angle between the

planes with the monomer C_3 axes and the bond axis **R**, it is not straightforward to extract this information. The expression for $\chi_{bb} - \chi_{cc}$ is an off-diagonal matrix element between the internal function $|\lambda, K\rangle$ and the interchanged function $\hat{I}^{ag}|\lambda, K\rangle$. If we define the angle $\gamma = \frac{1}{2}(\gamma_A + \gamma_B)$, which is an overall rotation angle of the dimer, and the dihedral angle $\bar{\gamma} = \gamma_A - \gamma_B$, we can substitute $\gamma_A = \gamma + \frac{1}{2}\bar{\gamma}$ and $\gamma_B = \gamma - \frac{1}{2}\bar{\gamma}$ into Eq. (31) and integrate over γ. Then, it is easy to show that $\chi_{bb} - \chi_{cc}$ in Eq. (31) can be written as the expectation value

$$\frac{1}{2}\sqrt{6} e Q q \langle C_2^{(2)}(\vartheta_A, \gamma_A) + C_2^{(2)}(\vartheta_B, \gamma_B) $$
$$+ C_{-2}^{(2)}(\vartheta_A, \gamma_A) + C_{-2}^{(2)}(\vartheta_B, \gamma_B)\rangle, \qquad (35)$$

with respect to the projected internal function $1/\sqrt{2}\,(\hat{E} + \hat{I}^{ag})|\lambda, K\rangle$. This follows, because the terms in Eq. (35) which are diagonal in $|\lambda, K\rangle$ and in $\hat{I}^{ag}|\lambda, K\rangle$ vanish and the two off-diagonal terms are equal. After substitution of the Racah spherical harmonics $C_\nu^{(2)}(\vartheta_A, \frac{1}{2}\bar{\gamma})$ and $C_\nu^{(2)}(\vartheta_B, -\frac{1}{2}\bar{\gamma})$ with $\nu = \pm 2$, it is found that

$$\frac{\chi_{bb} - \chi_{cc}}{eQq} = \frac{3}{2}\langle(\sin^2 \vartheta_A + \sin^2 \vartheta_B)\cos \bar{\gamma}\rangle. \qquad (36)$$

Still, we cannot directly extract information about the dihedral angle $\bar{\gamma}$ from this expectation value, because the integrations over ϑ_A, ϑ_B, and $\bar{\gamma}$ cannot be separated. If we would assume such a separation to hold, then we can calculate $\langle \sin^2 \vartheta_A + \sin^2 \vartheta_B \rangle$ from the expectation value $\langle P_2(\cos \vartheta_A) + P_2(\cos \vartheta_B) \rangle$ which was obtained from χ_{aa}. Thus we would find $\langle \cos \bar{\gamma} \rangle = -0.233$ from our calculated values of χ_{aa} and $\chi_{bb} - \chi_{cc}$ and $\langle \cos \bar{\gamma} \rangle = -0.334$ from our experimental data. For the calculated values this would yield an average $\bar{\gamma} \approx 104°$, whereas from the experiment it would follow that $\bar{\gamma} \approx 110°$. Since $\bar{\gamma} = 180°$, i.e., $\cos \bar{\gamma} = -1$, for the equilibrium structure of $(NH_3)_2$, this shows that the amplitude of the torsional motion in the calculations is larger than found experimentally. In other words, the potential of Olthof *et al.*[19] is too soft in its dependence on the dihedral angle $\bar{\gamma}$. The values given for $\bar{\gamma}$ must be regarded with caution, however. First, we could only obtain the expectation value in Eq. (35) by projection of the *internal* function with $\hat{E} + \hat{I}^{ag}$, whereas it is in fact the *total* wave function of $(NH_3)_2$ which must be projected with this operator, cf. Eq. (24). Secondly, one should remember that $\chi_{bb} - \chi_{cc}$ probes the dihedral angle $\bar{\gamma}$, *in combination with* the angles ϑ_A and ϑ_B, cf. Eq. (36). So we think that the values given for $\bar{\gamma}$ are only of qualitative importance, and that one should actually consider the "observable" $\chi_{bb} - \chi_{cc}$.

Finally, it should be noted that part of the discrepancy between the calculated and the observed value of $\chi_{bb} - \chi_{cc}$ might be due to the $\nu = \pm 1$ terms in q_J, cf. Table II, which are absent for the rigid rotor. The calculated value of $\chi_{bb} - \chi_{cc}$ has been obtained only from the rigid rotor like terms with $\nu = \pm 2$, cf. Eq (31), but in the fit of the experimental spectrum the nonvanishing $\nu = \pm 1$ contributions might enter implicitly into $\chi_{bb} - \chi_{cc}$. The E_4 state with

$|K| = J = 1$ and the E_3 state with $|K| = 1$ and $J = 2$ are strongly perturbed by Coriolis coupling to the nearby states with $K = 0$ and the resulting $\nu = \pm 1$ contributions to q_J are not negligible. Yet, it may be asserted as a conclusion from our calculations and measurements that the semiempirical potential of Olthof *et al.*[19] is very accurate in its dependence on the polar angles ϑ_A and ϑ_B, but probably too soft in its dependence on the dihedral angle $\bar{\gamma} = \gamma_A - \gamma_B$. With the new far-infrared data of Loeser[27] at frequencies between 80 and 90 cm^{-1}, which seem to probe explicitly the excitations in the angle $\bar{\gamma}$, it will be possible to improve this potential.

ACKNOWLEDGMENTS

[1] J.C. Dill, L.C. Allen, W.C. Topp, and J.A. Pople, J. Am. Chem. Soc. **97**, 7220 (1975).

[2] P. Kollman, J. McKelvey, A. Johansson, and S. Rothenberg, J. Am. Chem. Soc. **97**, 955 (1975).

[3] Z. Latajka and S. Scheiner, J. Chem. Phys. **81**, 407 (1984).

[4] M.J. Frisch, J.A. Pople, and J.E. Del Bene, J. Phys. Chem. **89**, 3684 (1985).

[5] M.J. Frisch, J.E. Del Bene, J.S. Binkley, and H.F. Schaefer, J. Chem. Phys. **84**, 2279 (1986).

[6] S. Liu, C.E. Dykstra, K. Kolenbrander, and J.M. Lisy, J. Chem. Phys. **85**, 2077 (1986).

[7] D.D. Nelson, G.T. Fraser, and W. Klemperer, J. Chem. Phys. **83**, 6201 (1985).

[8] D.D. Nelson, W. Klemperer, G.T. Fraser, F.J. Lovas, and R.D. Suenram, J. Chem. Phys. **87**, 6364 (1987).

[9] D.D. Nelson and W. Klemperer, J. Chem. Phys. **87**, 139 (1987).

[10] M. Havenith, R.C. Cohen, K.L. Busarow, D.-H. Gwo, Y.T. Lee, and R.J. Saykally, J. Chem. Phys. **94**, 4476 (1991).

[11] M. Havenith, H. Linnartz, E. Zwart, A. Kips, J.J. ter Meulen, and W.L. Meerts, Chem. Phys. Lett. **193**, 261 (1992).

[12] J.G. Loeser, C.A. Schuttenmaer, R.C. Cohen, M.J. Elrod, D.W. Steyert, R.J. Saykally, R.E. Bumgarner, and G.A. Blake, J. Chem. Phys. **97**, 4727 (1992).

[13] J.W.I. van Bladel, A. van der Avoird, P.E.S. Wormer, and R.J. Saykally, J. Chem. Phys. **97**, 4750 (1992).

[14] H. Linnartz, A. Kips, W.L. Meerts, and M. Havenith, J. Chem. Phys. **99**, 2449 (1993).

[15] D.M. Hassett, C.J. Marsden, and B.J. Smith, Chem. Phys. Lett. **183**, 449 (1991).

[16] F.-M. Tao and W. Klemperer, J. Chem. Phys. **99**, 5976 (1993).

[17] E.H.T. Olthof, A. van der Avoird, and P.E.S. Wormer, J. Mol. Struct. (THEOCHEM) **307**, 201 (1994).

[18] A. van der Avoird, E.H.T. Olthof, and P.E.S. Wormer, Faraday Discuss. Chem. Soc. **97**, 43 (1994).

[19] E.H.T. Olthof, A. van der Avoird, and P.E.S. Wormer, J. Chem. Phys. **101**, 8430 (1994).

[20] E.H.T. Olthof, A. van der Avoird, P.E.S. Wormer, J.G. Loeser, and R.J. Saykally, J. Chem. Phys. **101**, 8443 (1994).

[21] W. Gordy and R.L. Cook, *Microwave Molecular Spectra*, 3rd ed. (Wiley, New York, 1984).

[22] D.M. Brink and G.R. Satchler, *Angular Momentum*, 2nd ed. (Oxford, London, 1968).

[23] M.D. Marshall and J.S. Muenter, J. Mol. Spectrosc. **85**, 322 (1981).

[24] U. Andresen, H. Dreizler, J.-U. Grabow, and W. Stahl, Rev. Sci. Instrum. **61**, 3694 (1990).

[25] J.-U. Grabow and W. Stahl, Z. Naturforsch. Teil A **45**, 1043 (1990).

[26] A. van der Avoird, P.E.S. Wormer, and R. Moszynski, Chem. Rev. **94**, 1931 (1994).

[27] J.G. Loeser, Faraday Discuss. Chem. Soc. **97**, 159 (1994).